CORA Cork Open Research Archive
Cartlann Taighde Oscailte Chorcaí

Title	Nanoporous InP: anodic formation and growth mechanism in aqueous electrolytes
Authors	O'Dwyer, Colm
Publication date	2005-01-01
Original Citation	O'Dwyer, C. 'Nanoporous InP: anodic formation and growth mechanism in aqueous electrolytes', State-of-the-Art Program on Compound Semiconductors XLII -and- Processes at the Compound-Semiconductor/Solution Interface, 207th ECS Meeting, Quebec City, Canada, 15-20 May. Proceedings - Electrochemical Society, Vol. 4, pp. 40-63. ISBN 1-56677-462-4.
Type of publication	Article (peer-reviewed)
Link to publisher's version	http://www.electrochem.org/dl/pv/published/2005/2005.htm
Rights	© 2005, Electrochemical Society
Download date	2026-11-16 09:53:00
Item downloaded from	https://hdl.handle.net/10468/2880



UCC
University College Cork, Ireland
Coláiste na hOllscoile Corcaigh

NANOPOROUS InP: ANODIC FORMATION AND GROWTH MECHANISM IN AQUEOUS ELECTROLYTES

C. O'Dwyer [†]

Tyndall National Institute, Lee Maltings, Cork, Ireland

[†] Work performed in *Department of Physics, Materials and Surface Science Institute, University of Limerick, Ireland*

ABSTRACT

Porous layers can be formed electrochemically on (100) oriented n-InP substrates in aqueous KOH. A nanoporous layer is obtained underneath a dense near-surface layer and the pores appear to propagate from holes through the near-surface layer. In the early stages of the anodization transmission electron microscopy (TEM) clearly shows individual porous domains that appear to have a square-based pyramidal shape. Each domain appears to develop from an individual surface pit which forms a channel through this near-surface layer. We suggest that the pyramidal structure arises as a result of preferential pore propagation along the <100> directions. AFM measurements show that the density of surface pits increases with time. Each of these pits acts as a source for a pyramidal porous domain. When the domains grow, the current density increases correspondingly. Eventually the domains meet, forming a continuous porous layer, the interface between the porous and bulk InP becomes relatively flat and its total effective surface area decreases resulting in a decrease in the current density. Current-time curves at constant potential exhibit a peak and porous layers are observed to form beneath the electrode surface. The density of pits formed on the surface increases with time and approaches a plateau value. Porous layers are also observed in highly doped InP but are not observed in wafers with doping densities below ~5×10^{17} cm^{-3}. Numerical models of this process have been developed invoking a mechanism of directional selectivity of pore growth preferentially along the <100> lattice directions. Manipulation of the parameters controlling these curves shows that the fall-off in current is controlled by the rate of diffusion of electrolyte through the pore structure with the final decline in current being caused by the termination of growth at the pore tips through the formation of passivating films or some other irreversible modification of the pore tips.

INTRODUCTION

There is considerable interest in the electrochemical formation of porosity in semiconductors, both from the point of view of fundamental understanding and their applications. [1-7] Much of the work has focused on silicon but investigations of pore formation in III-V semiconductors such as GaAs [8-11] and InP [12-15] have also been reported. It has been suggested that controlled modulation of the pore diameter and pore

growth direction in such structures could lead to photonic crystals with a photonic band gap in the near infra-red or visible region. These characteristics are affected by electrolyte concentration [12,16,17], substrate type [18], orientation [19] and doping density. [20] Significant progress has been made in understanding the basic mechanisms of pore formation in silicon under electrochemical conditions, but only a limited number of investigations of the mechanism of pore formation in III-V semiconductors have been reported. For silicon, several pore formation models have been proposed to account for the variety of observed pore types [21-23]. We have recently reported [24] that both potentiodynamic and potentiostatic anodization in KOH electrolytes can result in the formation of a porous region below the surface of an InP electrode. The evidence strongly suggests that the porous layer structure arises from the penetration of pits into the surface at particular points and pore propagation within the InP originating at these points and proceeding along the <100> direction. [24] The electrolyte within the porous structure is connected to the bulk electrolyte by a limited number of surface pits which form channels through a dense near-surface layer, thus providing a mechanism by which the porous layer can grow. Consequently, these channels play a critical role in the evolution of the porous structure.

A subject of interest is the preferential orientation of the pore growth along specific crystallographic directions and how this leads to the development of a complete porous region within the semiconductor. In this paper we review our recent work on the formation of porous InP during anodization in KOH electrolytes. [25,26]

EXPERIMENTAL

The working electrode consisted of polished (100)-oriented monocrystalline sulfur doped n-InP with a carrier concentration of ~3×10^{18} cm^{-3}. For experiments conducted with wafers of different carrier concentrations, polished (100)-oriented monocrystalline sulphur-doped InP electrodes with carrier concentrations less than (n^--InP) and greater than (n^+-InP) the nominal (n-InP) carrier concentration were used. An ohmic contact was made by alloying indium to the InP sample and the contact was isolated from the electrolyte by means of a suitable varnish. The electrode area was typically 0.2 cm^2. Anodization was carried out in an aqueous KOH electrolyte at a concentration of 5 mol dm^{-3}. A conventional three electrode configuration was used employing a platinum counter electrode and saturated calomel reference electrode (SCE) to which all potentials are referenced. Prior to immersion in the electrolyte, the working electrode was dipped in a 3:1:1 H_2SO_4:H_2O_2:H_2O etchant and rinsed in deionized water. All of the electrochemical experiments were carried out at room temperature and in dark conditions. A CH Instruments Model 650A Electrochemical Workstation interfaced to a Personal Computer (PC) was employed for cell parameter control and for data acquisition.

Atomic force microscopy (AFM) studies were carried out with a ThermoMicroscopes Explorer AFM. Slices for plan view and cross-sectional microscopic analysis were prepared by thinning to electron transparency using standard focused ion beam milling procedures by means of a FEI 200 FIBSIMS workstation. The transmission electron microscopy (TEM) characterization was performed using a JEOL 2010 TEM operating at 200 kV.

RESULTS AND DISCUSSION

1. Formation of Porous InP in KOH

1.1 Electrochemical Formation of Porous InP

Fig. 1 shows a cyclic voltammogram of an n-InP electrode in a 5 mol dm^{-3} KOH. The potential was scanned at a rate of 2.5 mV s^{-1} from 0.0 V (E_i) to 0.68 V (E_{min}). At potentials less than 0.3 V (E_{pit}), very little current flow is observed, but continued anodization to potentials greater than 0.35 V results in a rapid increase in the current density from values less than 1 mA cm^{-2} below 0.35 V to a peak value of 20 mA cm^{-2} at 0.48 V (E_p). Above 0.48 V, the current density decreases quite rapidly, reaching a value of ~3 mA cm^{-2} at 0.6 V. Clearly, a significant anodic oxidation process occurs above 0.35 V and becomes self-limiting at higher potentials. It also observed that the current densities on the reverse sweep are much lower than the corresponding current densities on the forward sweep. This difference indicates that the rate of reaction is drastically reduced, reflecting effective passivation of the electrodes above E_p. A current peak is also observed when InP electrodes are anodized in other electrolytes.

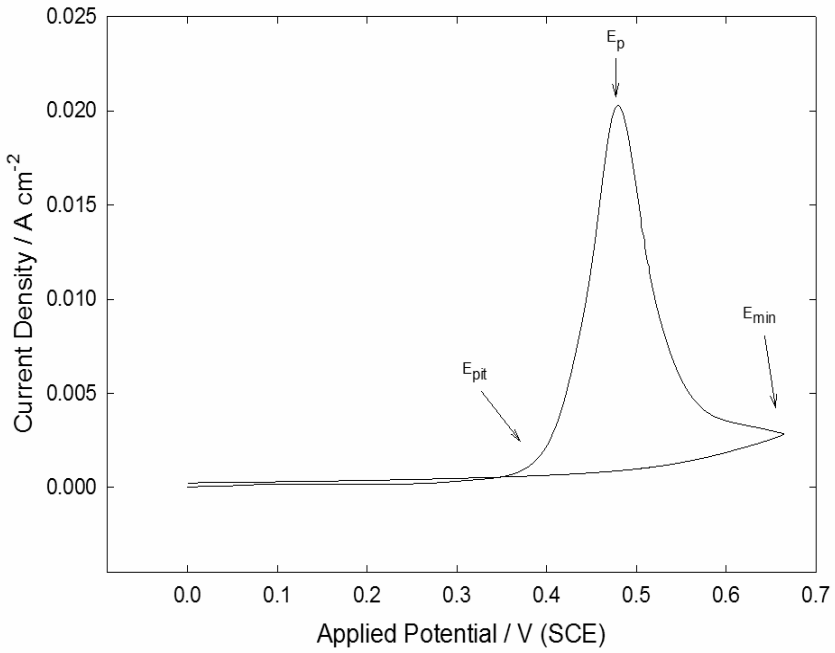


Fig. 1 Cyclic voltammogram of an n-InP electrode in a 5 mol dm^{-3} KOH electrolyte from 0.0 V to 0.68 V (SCE). The potential was scanned at a rate of 2.5 mV s^{-1}.

Cyclic voltammograms were obtained over a range of scan rates and upper potential limits. An anodic current peak is formed in all cases [27]. While the observed current densities are higher at the higher scan rates, the charge density corresponding to the anodic peak was found to remain relatively constant, (0.57 C cm^{-2}) indicating that an approximately equal amount of InP is oxidized irrespective of the scan rate. InP electrodes that had been subjected to a potential sweep such as that corresponding to the forward curve in Fig. 1 were cross-sectioned and analyzed using TEM in order to elucidate the type of process involved during the anodization. Fig. 2 is a cross-sectional TEM of an InP cross-section after a potential sweep at 2.5 mVs^{-1} from 0.0 V to 0.68 V in 5 mol dm^{-3} KOH. A region, marked (A), extending ~1 μm into the InP substrate (B), is

clearly modified and appears to be penetrated by a network of pores. However, a thin layer (~40 nm) close to the surface appears to be unmodified (C). The interface of the porous region and the substrate is generally relatively uniform, although in some areas it is somewhat non-planar. The average pore width and interpore distance are noted to be of similar value (~40 nm). Thus, the pore width and pore spacing are of similar thickness to the near-surface layer.

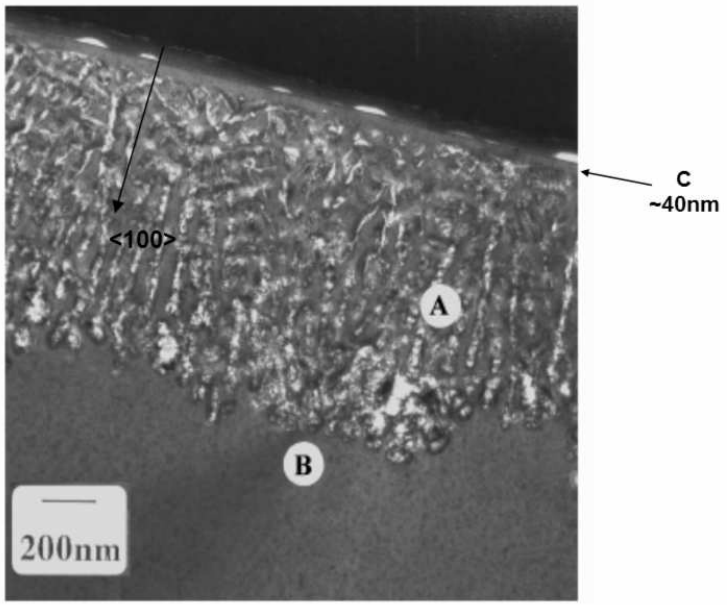


Fig. 2 Cross-sectional bright field through focal TEM of n-InP after a potential sweep from 0.0 V to 0.68 V (SCE) at a scan rate of 2.5 mV s^{-1} in 5 mol dm^{-3} KOH electrolyte. 'A' denotes the porous InP layer and 'B' denotes the InP substrate. The near-surface layer is shown at 'C'. The plane of the micrograph is (011).

The mechanism by which such a porous region can form by electrochemical oxidation of the substrate, despite the presence of this dense InP layer at the surface is not apparent from Figs. 2 and 3. Closer examination by TEM reveals that the dense, near-surface layer is penetrated at certain points by narrow channels. The TEM micrograph in Fig. 3 shows a higher magnification cross-section of an electrode subjected to the same anodization procedure as that described for Fig. 2.

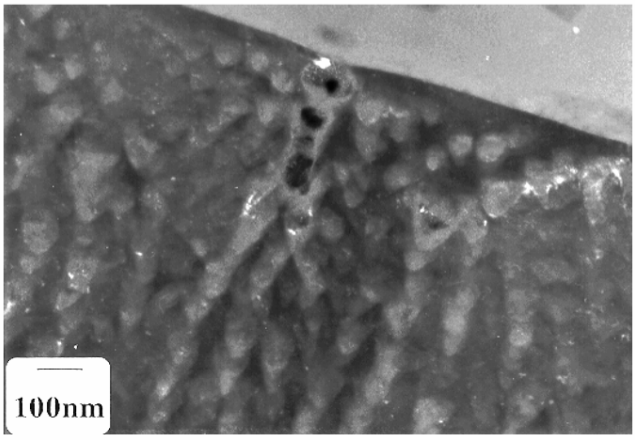


Fig. 3 Dark Field cross-sectional TEM of the InP electrode described in Fig. 2 showing a channel through the near-surface layer. The plane of the micrograph is (011).

It can be observed that the dense, near-surface layer appears to be penetrated at one point by a channel. The texture of the porous layer suggests that the pores emanate from this point in the near-surface layer which suggests a mechanism by which the porous layer can grow, *i.e.* it appears to be connected to the electrolyte by channels through the near-surface layer. Further evidence for the existence of these pores was obtained from AFM measurements of the surface of electrodes. Careful AFM examination of the surface of wafers such as that represented in Fig. 4 shows the presence of pits in the surface. These AFM results are discussed in detail in the section 1.2.

1.2 AFM Studies of Surface Morphology and Pitting

AFM was employed to characterize the surface of the InP electrodes after anodization in KOH electrolytes. Electrodes subjected to potential sweep anodization with upper potentials in the range 0.4 V to 0.53 V were studied by AFM. Fig. 4a shows an AFM image of the surface of an InP electrode that was subjected to a potential sweep at 2.5 mV s^{-1} from 0.0 V to 0.425 V in 5 mol dm^{-1} KOH. The image clearly shows an etch pit which has formed on the surface. Similar pits were observed in AFM images obtained for potential sweep experiments at other upper potentials in the range 0.4 V to 0.53 V. For example, an image obtained for an upper potential of 0.48 V (*i.e.* at the current peak) is shown in Fig. 4b. Although the AFM cannot measure the diameter of deep pits, we can obtain some estimate of the diameter of the pits from line traces through the pit centers. Thus, taking the value of the full width at half maximum from these traces we obtain a value of ~50 nm for the pore diameter, in good agreement with observations in cross-sectional TEM images. No pits were observed on surfaces anodized between 0.0 V and 0.35 V.

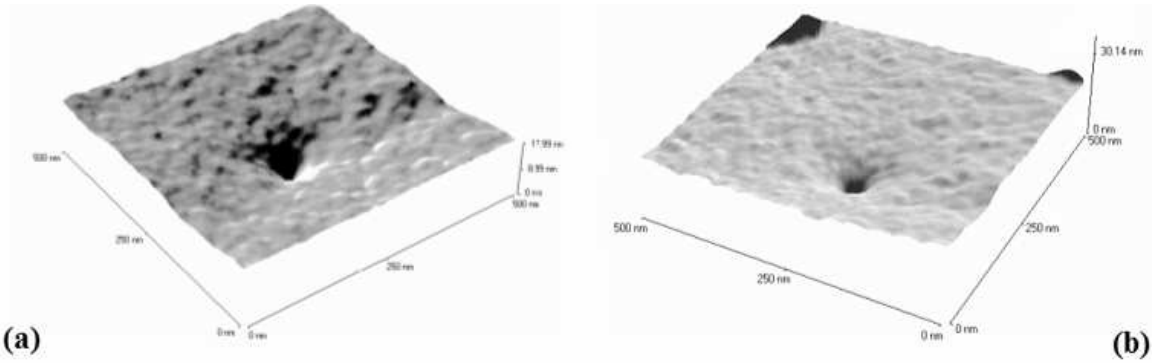


Fig. 4 AFM images of the InP surface after potential sweep anodization at 2.5 mV s^{-1} in 5 mol dm^{-3} KOH from 0.0 V to (a) 0.425 V, (b) 0.48 V.

Estimates were made of the areal density of pits on electrode surfaces after anodization under potentiodynamic conditions. A series of experiments was carried out in which electrodes were subjected to potential sweeps at 2.5 mV s^{-1} from 0.0 V to upper potentials in the range 0.48 V to 0.68 V and 10 μm × 10 μm AFM images were obtained of the resulting surfaces. A typical such image is shown in Fig. 5a for an upper potential of 0.48 V (corresponding to the current peak). At this lower magnification, multiple pits are visible on the surface. By counting the pits (~23 for this image) we can estimate the areal density of pits on the surface (2.3×10^7 cm^{-2} in this case). Estimates of pit density were similarly obtained for electrodes anodized to various upper potentials and average values of pit density were obtained in each case. A similar study was conducted on the surfaces of electrodes subjected to constant potential anodization at 0.5 V. AFM images

were obtained at anodization times in the range 5 – 40 s and a typical image of the surface after anodization for 25 s is shown in Fig. 5b. Details of the variation of pit density with upper potential for electrodes anodized under potential sweep conditions and for various times for electrodes anodized under constant potential conditions will be outlined in section 2.1. Thus, it is suggested that the pitting of the surface allows for the continued preferential etching of the InP by providing a pathway for electrolyte to the tips of advancing sub-surface pores.

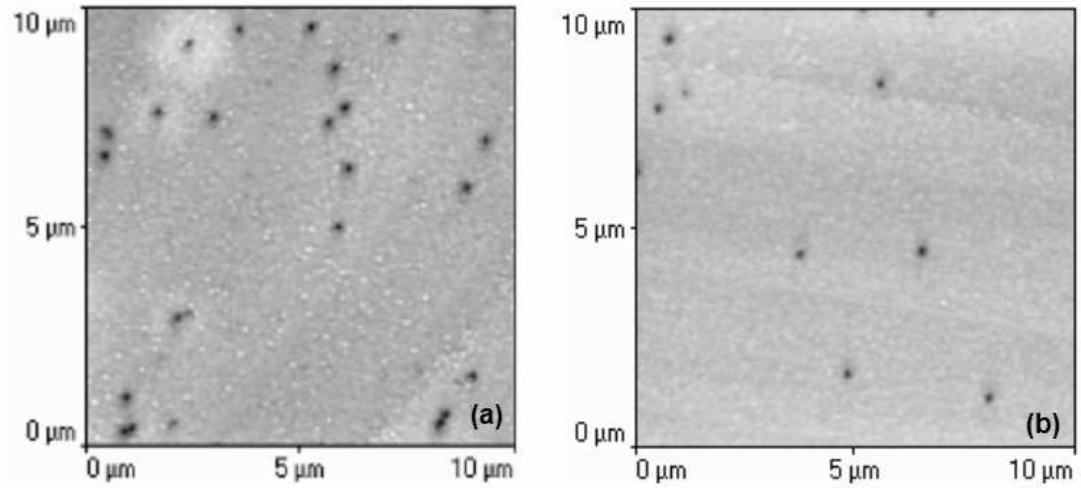


Fig. 5 AFM image of the surface of an InP electrode surface after (a) potential sweep anodization from 0.0 V to 0.48 V at 2.5 mV s^{-1} and (b) constant potential anodization at 0.5 V for 25 s in 5 mol dm^{-3} KOH.

1.3 Effect of Electrolyte Concentration

Experiments were also carried out at lower concentrations of KOH. Fig. 6 shows linear potential sweeps of InP electrodes in 2 mol dm^{-3} and 3 mol dm^{-3} KOH electrolytes under similar conditions to that outlined in Fig. 1. The potential was scanned at a rate of 2.5 mV s^{-1} with an initial potential of 0.0 V. The overall response in Fig. 6 is very similar to what is observed in 5 mol dm^{-3} under similar conditions; anodic current peaks are observed. Cross-sectional TEM confirms that the anodic currents in these electrolytes also correspond to the formation of porous layers. This evidence can be seen in Fig. 7 which shows the cross-sections of electrodes that had been subjected to potential scans from 0.0 V to 0.825 V in 2 mol dm^{-3} KOH and from 0.0 V to 0.675 V in 3 mol dm^{-3} KOH respectively. In each case, a porous layer similar to that obtained in 5 mol dm^{-3} KOH is clearly observed. Again, closer examination reveals the existence of a thin, dense, near-surface layer in each case, which is penetrated in places by pores.

1.4 Potentiostatic Anodization in 2 - 5 mol dm^{-3} KOH

Experiments were also carried out at constant potential. In a series of experiments in 5 mol dm^{-3} KOH, the potential was stepped from open circuit to potential values in the range 0.5 – 0.75 V. These potentials correspond to potentials on a typical current-voltage curve where porous layer formation is observed. Fig. 8 shows the current-time curves obtained for InP electrodes anodized in 5 mol dm^{-3} KOH at potentials of 0.5 V, 0.6 V and 0.75 V respectively for 100 s.

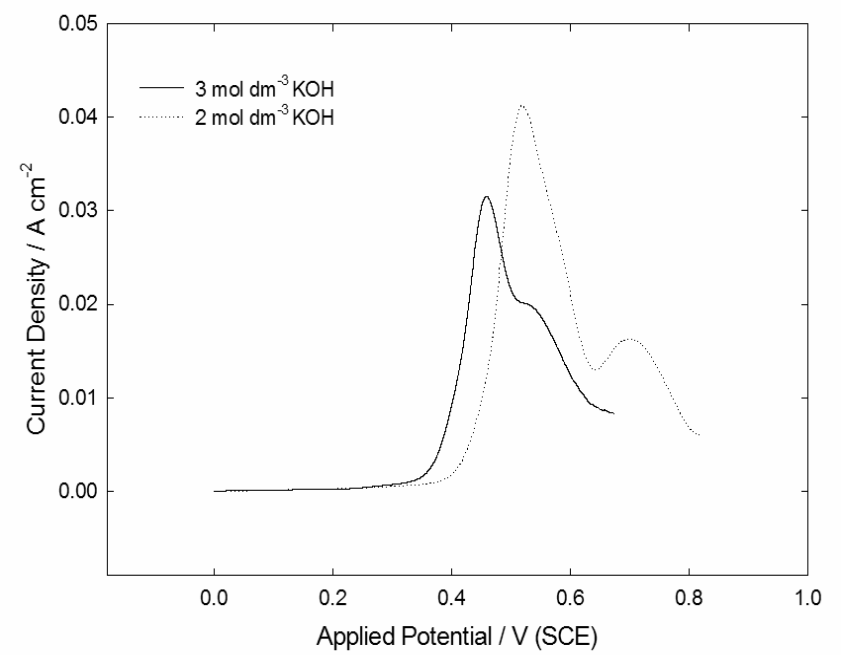


Fig. 6 Linear potential sweeps of InP electrodes in (a) 3 mol dm^{-3} KOH from 0.0 V to 0.675 V and (b) 2 mol dm^{-3} KOH from 0.0 V to 0.825 V. The data was acquired at a scan rate of 2.5 mV s^{-1}.

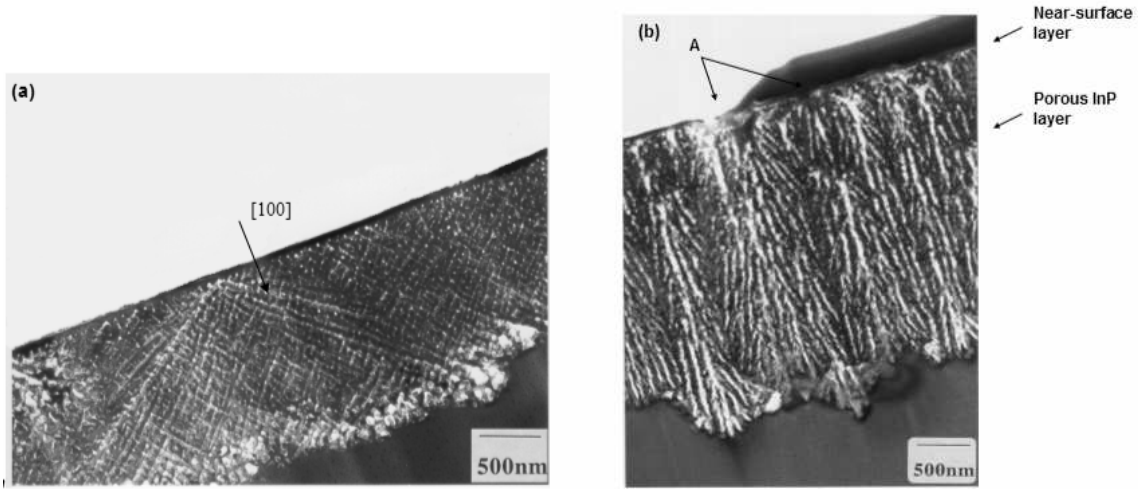


Fig. 7 Bright field cross-sectional TEM of InP after (a) potential sweep from 0.0 V to 0.825 V (SCE) in 2 mol dm^{-3} KOH (b) after a potential sweep from 0.0 V to 0.675 V (SCE) in 3 mol dm^{-3} KOH. The scan rate was 2.5 mV s^{-1}. The plane of both micrographs is (011).

The current initially increases with time in each case, reaching a peak after 23, 8 and 5 s respectively and subsequently decreases. It is observed that the peak current density increases with increasing applied potential, but the time taken for the current density to reach its maximum value decreases with increasing potential. This type of current-time curve is typically observed where a nucleation process is occurring. Cross-sectional TEM examination was carried out on electrodes anodized at each of the potentials in Fig. 8, *i.e.* 0.5 V, 0.6 V and 0.75 V. The images obtained are shown in Refs. 25 and 26 and are found to be very similar to those found in potentiodynamically anodized samples.

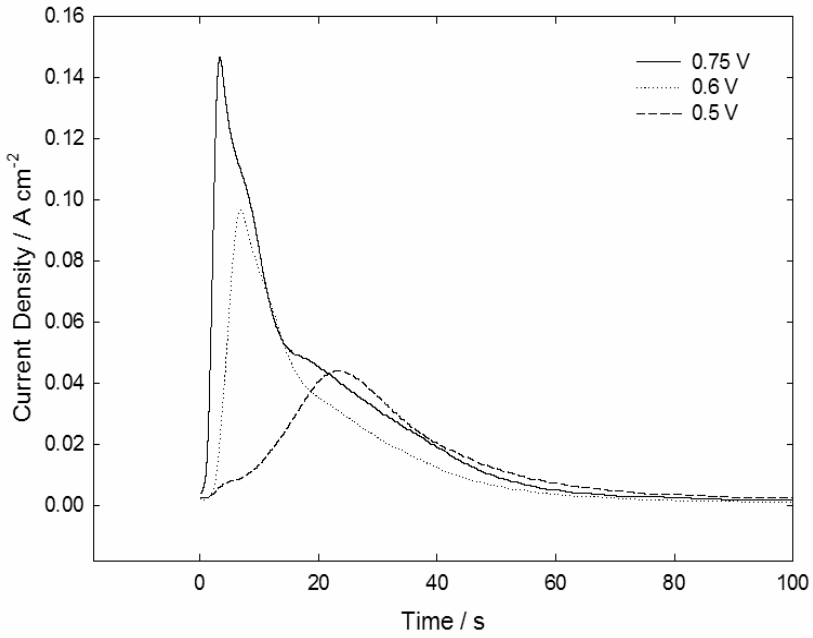


Fig. 8 Current-time curves for InP anodized in 5 mol dm^{-3} KOH in dark conditions at room temperature at bias potentials of (a) 0.5 V, (b) 0.6 V and (c) 0.75 V for 100 s.

The porous layer formed at 0.75 V is ~3 μm in thickness, twice a thick as the layers formed at 0.5 V and 0.6 V. Again channels through the near-surface layer are observed. Examples can be seen in Fig. 9 which shows a high resolution dark-field image of the sample anodized at 0.75 V.

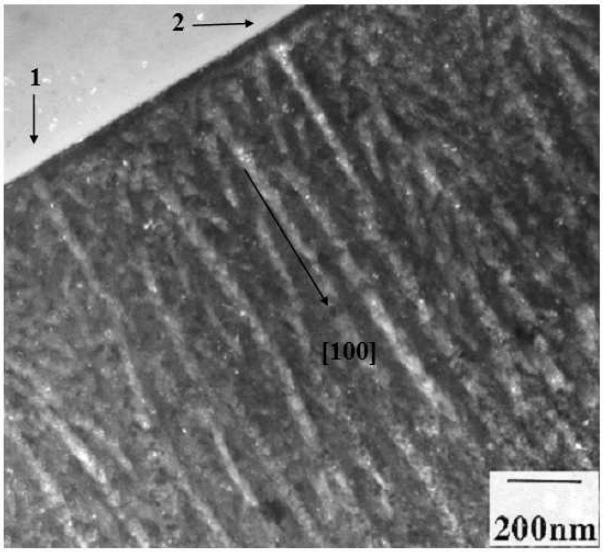


Fig. 9 Dark field through focal TEM of n-InP after constant potential anodization at 0.75 V (SCE) for 100 s in 5 mol dm^{-3} KOH. The plane of the micrograph is (011).

Experiments were also carried out at lower concentrations of KOH. Typical current-time curves of InP electrodes polarized at 0.75 V in 2 mol dm^{-3} and 3 mol dm^{-3} KOH solutions are shown in Fig. 10. Cross-sectional TEM confirms that the anodic currents in these electrolytes also correspond to the formation of porous layers. This can

be seen in Figs. 11a and 11b which show the cross-sections of electrodes which had been subjected to anodization at a constant potential of 0.75 V for 150 s in 2 mol dm^{-3} KOH and 3 mol dm^{-3} KOH respectively. In each case, a porous layer similar to that obtained in 5 mol dm^{-3} KOH is clearly observed. Again, closer examination reveals the existence of a thin, dense, near-surface layer in each case.

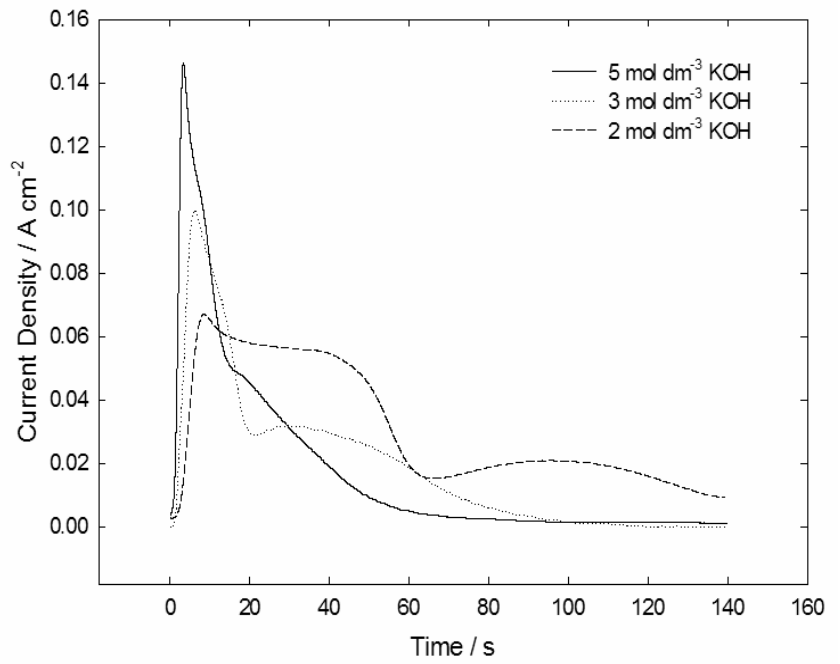


Fig. 10 Current-time curves for InP anodized in (a) 2 mol dm^{-3} (b) 3 mol dm^{-3} and (c) 5 mol dm^{-3} KOH in dark conditions at room temperature at a constant potential of 0.75 V for 150 s.

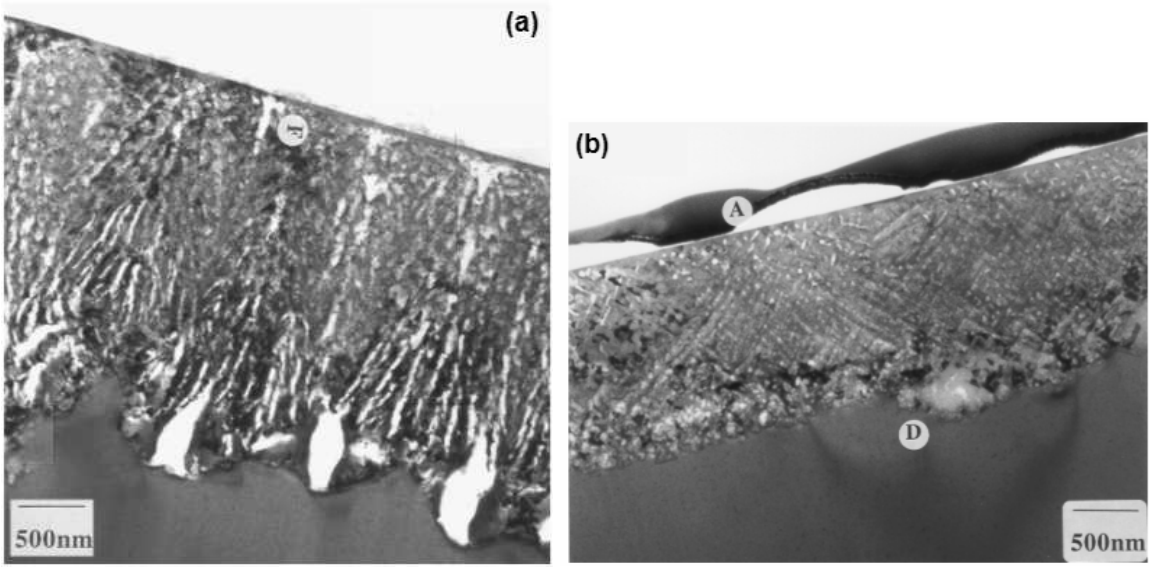


Fig. 11 Cross-sectional bright field TEM micrograph of an n-InP electrode after anodization at a constant potential of 0.75 V (SCE) in (a) 2 mol dm^{-3} KOH and (b) 3 mol dm^{-3} KOH for 150 s in dark conditions.

1.5 Characteristics of the Porous Region

The average thickness of the porous layers formed in 2, 3 and 5 mol dm^{-3} KOH electrolytes after a potential sweep from 0.0 V to 0.825 V, 0.675 V and 0.7 V respectively at 2.5 mV s^{-1} was estimated from TEM micrographs of electrode cross-sections. The mean pore width was also estimated from higher magnification micrographs of each porous layer. This estimation was done by drawing a series of lines on the micrograph and estimating the width of each pore through which the lines passed. The dependence of the porous layer thickness and mean pore diameter on the electrolyte concentration is shown in Fig. 12a. It is clear that both the porous layer thickness and mean pore diameter decrease significantly with increasing concentration of KOH. Estimates of porous layer thickness and mean pore width were also obtained for samples potentiostatically anodized at 0.75 V. These estimations were also acquired for 2, 3 and 5 mol dm^{-3} KOH in the same manner as that described for Fig. 12a and the estimates are plotted in Fig. 12b.

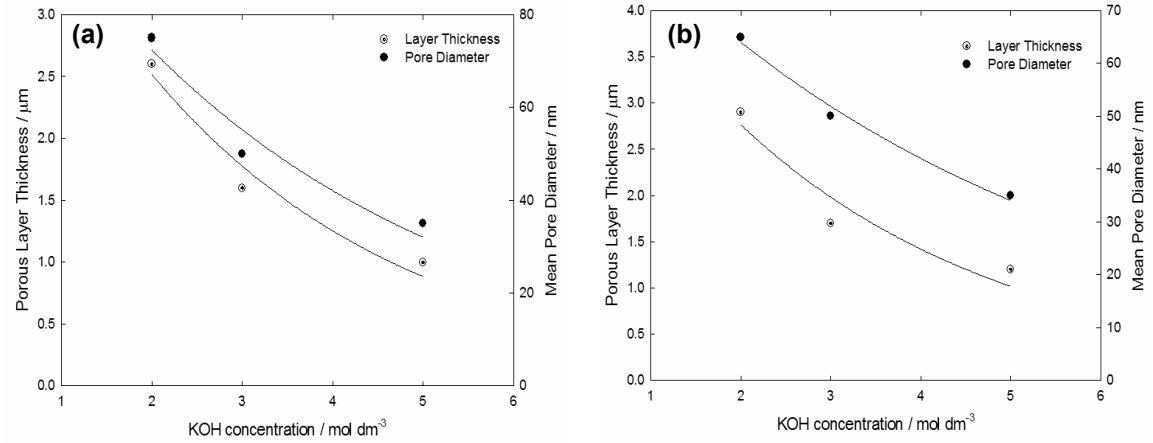


Fig. 12 Plots of the porous layer thickness (circles) and mean pore diameter (squares) for n-InP electrodes after (a) potential sweep at a scan rate of 2.5 mV s^{-1} from 0.0 V to 0.825 V, 0.675 V and 0.7 V in 2, 3 and 5 mol dm^{-3} KOH and (b) after constant potential anodization at 0.75 V in 2, 3 and 5 mol dm^{-3} KOH respectively for 150 s.

It is observed that an increase in KOH concentration results in a decrease in both the pore diameter and the porous layer thickness, in a similar manner to what was noted in Fig. 12a for porous layers formed under potential sweep anodization. For each of the samples mentioned for which the thickness of the porous layer was measured, the corresponding charge density passed was also estimated. This charge density estimation was accomplished by estimating the integral of current with respect to time. The measured thickness of the porous layer was then plotted against the corresponding charge density. The results are shown in Fig. 13. It is clear that a reasonable fit to a straight line though the origin is obtained. The slope of this line gives a value of 1.13 μm C^{-1} cm^2 for the ratio of porous layer thickness to charge density (Fig. 13a). The observation that the porous layer thickness increases approximately in proportion to charge density indicates that a relatively constant percentage porosity is maintained. A theoretical value for the ratio of layer thickness to charge density passed was also estimated. Using Faraday's law, the ratio of the thickness, d, of InP oxidized to the charge density, Q, is given by the equation

$$\frac{d}{Q} = \frac{V_{M(InP)}}{nF} \qquad (1)$$

where $V_{M(InP)}$ is the molar volume of InP, n is the number of electrons per formula unit of InP and F is the Faraday constant.. Using a value [27] of 30.31 cm^3 mol^{-1} for $V_{M(InP)}$ and assuming n = 8, a theoretical value of 0.393 μm C^{-1} cm^2 is estimated from Eqn. 1 for d/Q, the ratio of layer thickness to charge density for complete removal of InP. This theoretical ratio is represented by line (b) in Fig. 13. As indicated above, the slope of line (a) provides an estimate of 1.13 μm C^{-1} cm^2 for the corresponding ratio d_e/Q of experimental porous layer thickness d_e to charge density. The ratio of these estimates of d/Q and d_e/Q gives a value of $r = d/d_e = 0.347$, *i.e.* the estimated thickness of a compact InP layer, which represents the quantity of InP removed, is a fraction $r = 0.347$ of the corresponding as-measured porous layer thickness. Thus, the porosity of the porous layers formed on InP after anodization in KOH electrolytes is ~35%.

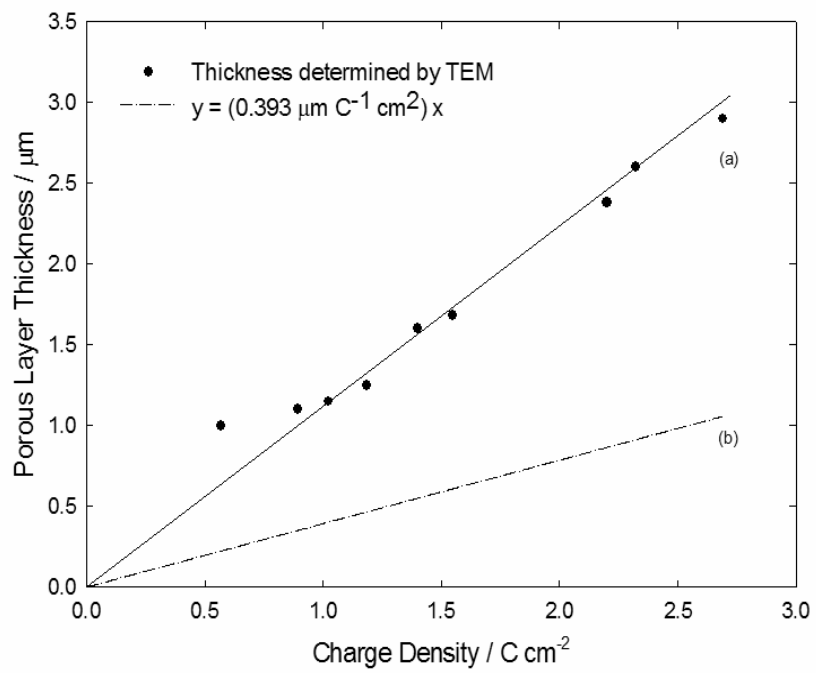


Fig. 13 (a) Plot of porous layer thickness for samples anodized at constant potential and after potential sweep as a function of the charge passed. (b) Theoretical thickness of InP removed.

1.6 Effect of Carrier Concentration

Experiments were carried out on wafers with carrier concentrations greater than (n^+-InP) and less than (n^--InP) the typical value (n-InP) used in earlier experiments. Each was subjected to a linear potential sweep at 2.5 mV s^{-1} from an initial potential of 0.0 V. The resulting voltammograms are shown in Fig. 14. In comparison with the n-InP (shown in Fig. 14 for comparison), it is clear that the n^+-InP wafer gives a similar current peak but at a considerably lower potential. The peak current density (24 mA cm^{-2}) is slightly higher than in the case of the n-InP (20 mA cm^{-2}) and the corresponding charge density is 0.86 C cm^{-2} for the n^+-InP as compared with 0.57 C cm^{-2} for the n-InP. In the case of the n^--InP, however, a very much smaller anodic peak is obtained (peak current density of ~0.1 mA cm^{-2} and charge density of 0.012 C cm^{-2}) at a potential of 0.64 V. After anodization, cross-sectional TEM examination of each of the electrodes was carried out. Fig. 15 is a bright field TEM micrograph of the cross-section of the n^+-InP electrode after a potential

sweep from 0.0 V to 0.3 V. It is clear that a porous region has been formed beneath a thin near-surface layer, as has been observed for the n-InP wafers discussed earlier.

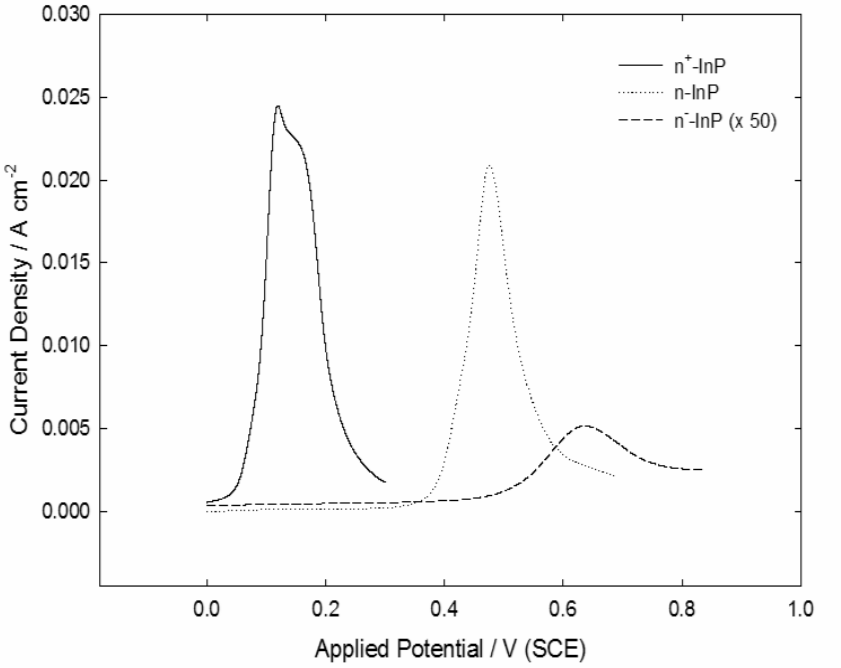


Fig. 14 Linear sweep voltammograms of n^+-InP and n^--InP electrodes in 5 mol dm^{-3} KOH in dark conditions at room temperature at a scan rate of 2.5 mV s^{-1}. The current-voltage response of the lower doped sample was magnified by 50 for clarity.

The texture of the porous region appears to be generally similar to that obtained for an n-InP electrode after potential sweep anodization (Fig. 2). However, the thickness of the near-surface layer is ~25 nm for the n^+-InP as compared with ~40 nm for the n-InP. Similarly, both the pore width and the interpore distance appear to be somewhat smaller (~25 nm) in the case of the n^+-InP as compared with the n-InP (~40 nm).

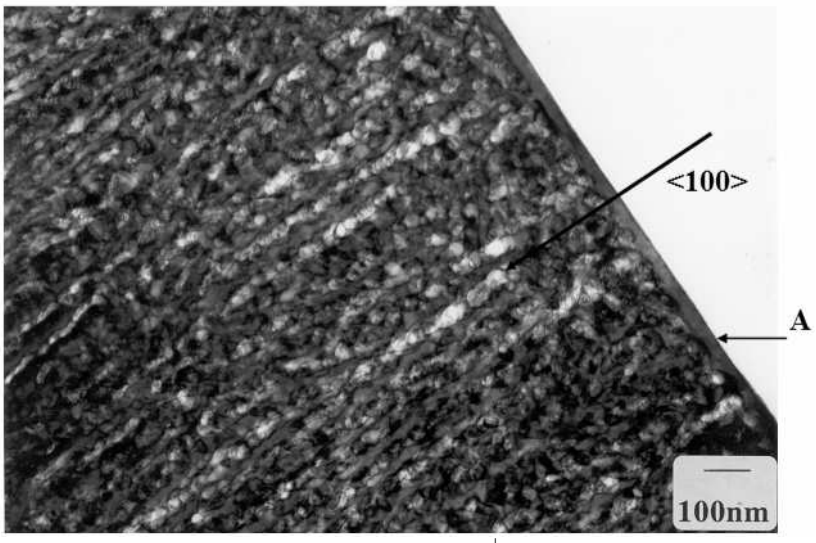


Fig. 15 Bright field through focal TEM of an n^+-InP electrode after potential sweep anodization at 2.5 mV s^{-1} in 5 mol dm^{-3} KOH from 0.0 V to 0.3 V. The plane of the micrograph is (011). A near surface layer is seen at 'A'.

The thickness of the porous region in the case of the n^+-InP, as determined from lower magnification micrographs of the entire layer is ~1.6 μm in comparison with ~1 μm in the case of n-InP (Fig. 2). Comparing the total charge for the respective anodic peaks (0.86 C cm^{-2} for n^+-InP and 0.57 C cm^{-2} for n-InP from Fig. 14), it is clear that the layer thickness scales approximately with the charge density and so the porosity is expected to be similar in both cases. In sharp contrast with n^+-InP and n-InP, cross-sectional TEM reveals no porous region for the n^--InP electrode described in Fig. 14. This is consistent with the observation of a very small anodic peak in Fig. 14 and a correspondingly lower charge density. The current densities measured for such samples are ~200 times lower than those measured for n-InP samples under identical conditions.

2. Mechanistic Study of Porous InP Formation

2.1 Pitting of the InP Surface

As reported in section 1.2, pitting of the InP surface occurs at potentials corresponding to the rising portion of the current-voltage curve when InP electrodes are anodized in KOH electrolytes of concentrations greater than 2 mol dm^{-3}. It was shown in sections 1.1 and 1.2 that these surface pits are actually channels through the near-surface layer when viewed in cross-section and thus play an integral role in the formation of the sub-surface porous layer. The variation in areal density of surface pits under constant potential and potential sweep anodization was investigated in detail using AFM. Estimates of pit density were obtained by determining the average number of pits on a 10 μm × 10 μm square area of the electrode. This was done for a range of upper potentials and the results are plotted in Fig. 16a.

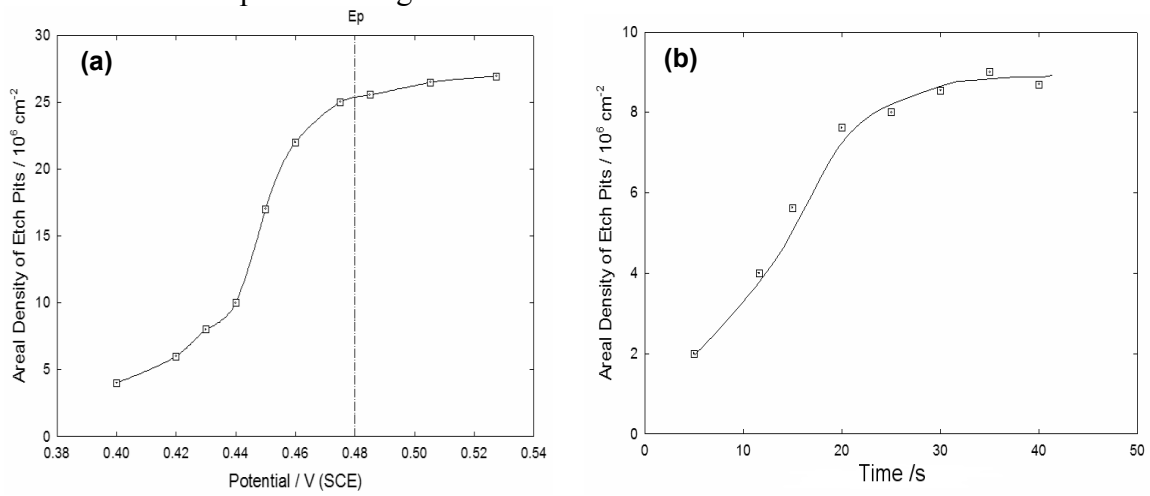


Fig. 16 Surface pit density, as determined by AFM, (a) plotted as a function of the upper potential limit of the potential sweep where the scan rate was 2.5 mV s^{-1} and (b) as a function of anodization time at a potential of 0.48 V. The electrolyte was 5 mol dm^{-3} KOH,

It is clear that the density of pits on the surface increases progressively with increasing potential. The rate of increase is greatest in the vicinity of 0.45 V. This corresponds to half the peak current on the low-potential side of the peak in the forward current-voltage curve, seen in Fig. 1 in section 1.1. Above ~0.48 V (*i.e.* the potential of

peak current) the pit density begins to plateau and further increase in pit density is small. Thus, the observed increase in density of pits corresponds to the onset of the anodic peak.

AFM studies were also conducted on electrode surfaces subjected to potentiostatic anodization. InP electrodes were anodized at 0.48 V for times ranging from 5 s to 40 s and AFM images of the surfaces were obtained. Values of pit density obtained from such images are plotted as a function of anodization time in Fig. 16b. It is observed that the density of pits formed on the surface increases with time and approaches a plateau value after 20 – 30 s. Thus, surface pitting at constant potential develops in a similar manner to that observed under potential sweep conditions and is a progressive process. Thus, the channels formed in the near-surface layer, which are believed to be the pathways for electrolyte to the pores form progressively in time and, as it will be shown, this progressive nucleation of surface pits influences the overall growth mechanism of the sub-surface porous layer.

2.2 Mechanism of Porous InP Formation

In order to investigate the mechanism by which porosity develops in InP under anodic conditions in KOH, experiments were carried out in which the potential was swept from 0.0 V to 0.44 V and the electrode was then cross-sectioned and examined. A TEM micrograph of such a cross-section is shown in Fig. 17a. This micrograph shows that, at this stage of the anodization, individual porous regions had formed that have a triangular cross-section with the base of the triangle parallel to the InP surface. As was observed for the more fully developed porous layer (Fig. 2 in section 1.1) the triangular porous region is separated from the surface by a thin non-porous near-surface layer. The measured thickness of this layer in Fig. 17a is ~40 nm. The cross-section in Fig. 17a is along the (011) plane. By symmetry we would expect a similar cross-section along the perpendicular (011) plane, which suggests that the porous region in Fig. 17a has a square-based pyramidal structure. Supplementary investigation was also carried out by plan-view TEM observation of the electrode. Fig. 17b shows a TEM micrograph of a slice through the InP in the (100) plane, parallel to the surface and ~100 nm below it. A porous region with an approximately square outline is clearly visible, consistent with a square based pyramidal structure for the porous region as suggested above.

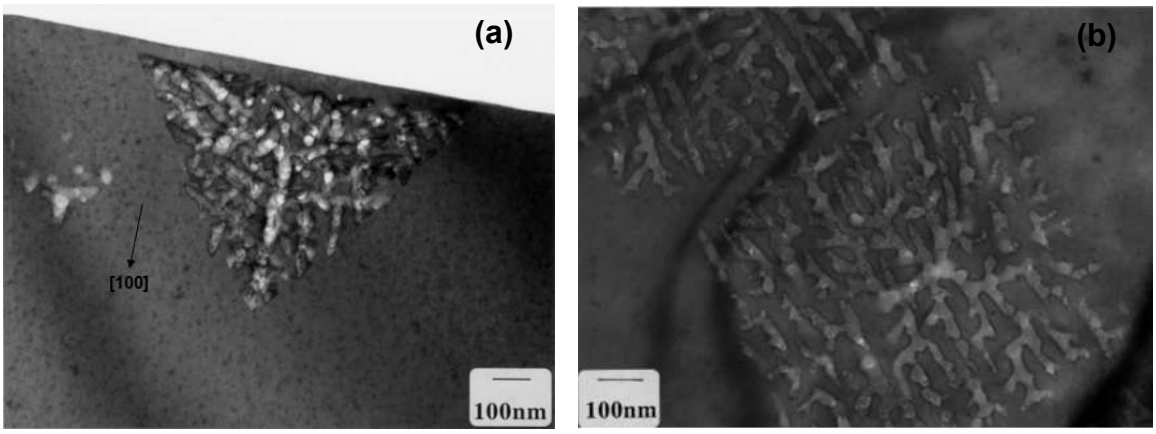


Fig. 17 (a) Dark Field cross-sectional TEM of the InP electrode described in Fig. 2 showing a channel through the near-surface layer. (b) Plan view bright field TEM image of a section through a porous InP layer ~100 nm below the surface of the electrode. The plane of the micrograph is (100). Nearby porous domains are visible.

We suggest that each pyramidal porous structure formed corresponds to a single channel through the near-surface layer. We further suggest that the pyramidal structure arises as a result of preferential pore propagation along the <100> directions. We postulate that each pyramidal structure grows by a process whereby all pore tips in a particular structure are advancing with equal speed. We now show that such a growth mechanism leads to the type of square based pyramidal porous domains observed.

To facilitate discussion of the growth of an individual pyramidal porous structure, we define cartesian co-ordinates as follows. We define a *y*-axis along the [100] direction (*i.e.* normal to the surface of the electrode), an *x*-axis along the [010] direction and a *z*-axis along the [100] direction. The origin (0,0,0) is defined as the bottom of the channel through the near-surface layer. This is depicted in Fig. 18.

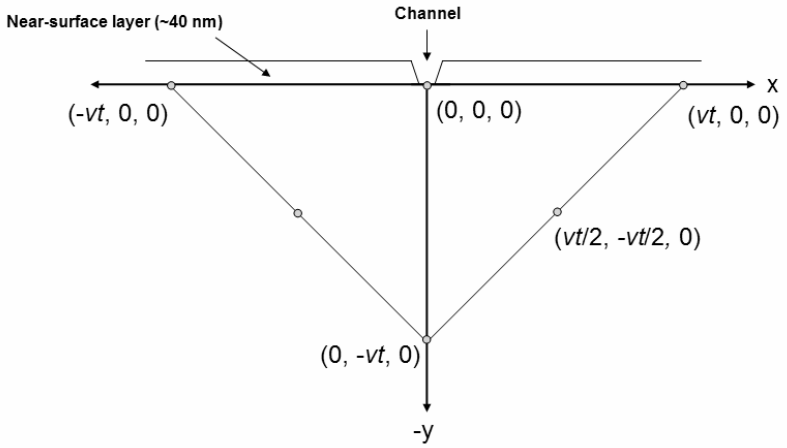


Fig. 18 Definition of cartesian co-ordinates for an individual porous region. The *y*-axis is normal to the electrode surface and the *z*-axis is out of the plane of the page. The origin is at the bottom of a channel through the near-surface layer as shown.

Consider a pore propagating from the origin. It can propagate in any of five directions, namely -*y*, *x*, -*x*, *z* and -*z*. Assume that the pore is propagating at some speed *v*. If it propagates along the -*y* direction it will reach a point with co-ordinates (0, -*v*t 0) a distance *v*t below the surface layer at time t. Similarly, if it propagates along the *x* direction it will reach a point (*v*t, 0, 0) just underneath the near-surface layer. If the pore propagates for time t/2 along the -*y* direction and then branches and travels for time t/2 along the *x* direction, it will reach a point (*v*t/2, -*v*t/2, 0) at time t. In fact, if the pore propagates along any combination of paths along the -*y* direction and the *x* direction it will reach a point on the line joining (0, -*v*t, 0) and (*v*t, 0, 0). Likewise, a pore propagating by any combination of paths along the -*y* direction and the -*x* direction will reach a point on the line joining (0, -*v*t, 0) and (-*v*t, 0, 0), at time t. Similarly, pores propagating along paths involving the -*y* direction in combination with the *z* direction and the -*z* direction will reach, at time t, points on the lines joining (0, -*v*t, 0) to (0, 0, *v*t) and (0, 0, -*v*t) respectively. Extending the argument to combinations of paths involving all three axes, it is clear that pores propagating in this way will reach, at time t, points on the surface of a square based pyramid defined by the above-mentioned four line segments and the plane of the bottom of the near-surface layer.

The structure and shape of the porous domain was analyzed further. In Fig. 19, a three-dimensional schematic of the cross-section is shown, where $h = vt$, *i.e.* h is the total length that a pore can propagate. Fig. 19 is drawn in three dimensions for clarity to emphasize the characteristic lengths corresponding to the width and depth of the porous

domain. The structure is defined as follows: the central pore that propagates in the [100] direction from directly beneath the channel in the near-surface layer grows to a length *h*.

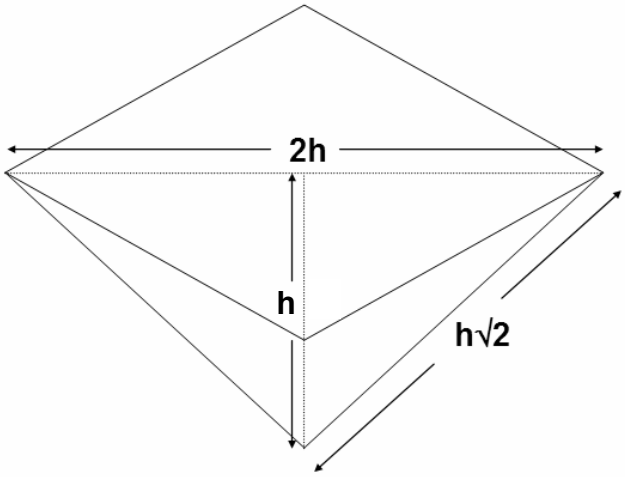


Fig. 19 3-D schematic representation of the porous domain. The total length of a pore from its source at the channel in the near-surface layer to the tip is $h = vt$.

A pore that branches in a lateral <100> direction orthogonal to this central pore immediately below the near-surface layer will also grow a distance *h*. Thus the width of the porous domain at its widest point (just below the near-surface layer) is 2*h*. By symmetry, we obtain a similar chracteristics for the (010) plane. The base of each of these triangles corresponds to a diagonal of the base of the pyramid, which is in the (100) plane (corresponding to a plan view parallel to the surface of the electrode). This view is shown in Fig. 20a. The diagonal represents the width of the porous domain when viewed in the (001). The side of the square is $b = h\sqrt{2}$ and this is the width of the domain as viewed in a (011) projection. The (001) and (011) projections are indicated in the diagram. Such a (011) projection through the center of the pyramid is shown schematically in Fig. 20b. For this projection, the height will be *h*, *i.e.* it will have the same height as the (001) projection in Fig. 19.

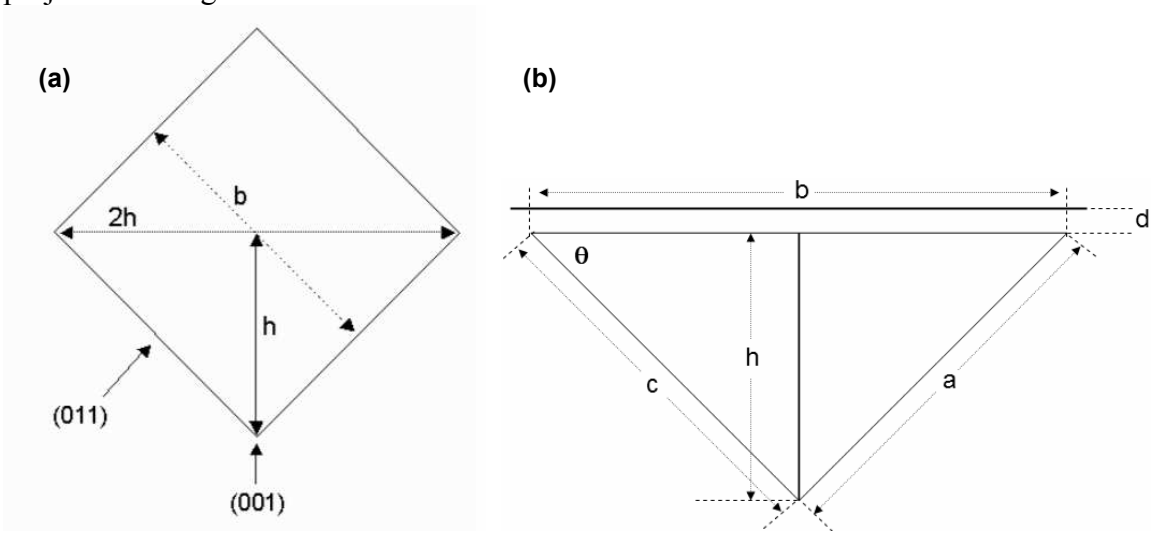


Fig. 20 Schematic representation of (a) plan view and (b) the (011) projection of the porous domain. The base of the triangle is a distance *d* below the surface of the InP representing the thickness of the near-surface layer. The length of the base is *b*, the lengths of the sides are *a* and *c* respectively.

Thus the predicted value of the width-to-depth ratio is $b/h = h\sqrt{2}/h = \sqrt{2} = 1.414$. Similarly, the ratio, $b/a = 1.15$, where a is the side of the triangle shown in Fig. 20b. The (011) cross-section represented in Fig. 20b may be compared with the experimentally observed (011) cross-section shown in Fig. 17a. It can be seen that there is excellent agreement between the ratios predicted by the model and the experimental values.

Thus, there is strong evidence that the porous region grows with the formation of square based pyramidal domains such as would result from the propagation of pores that all have, at an instantaneous point in time, equal pore front velocity along the <100> directions. As discussed earlier, AFM examination of the surfaces of electrodes subjected to anodic potential sweeps such as that in Fig. 1 in section 1.1, show a distribution of pits on the surface the density of which increases progressively with increasing upper potential, as outlined in Fig. 16. Similarly, AFM examination has also shown that the density of surface pits increases with time at a constant potential of 0.5 V. It is postulated, as stated earlier, that each of these pits acts as a source for a pyramidal porous domain, and these domains eventually form a continuous porous layer. This postulation implies that the development of porous domains beneath the surface is also progressive in nature. Evidence for this can be seen in the (100) plan view TEM images in Fig. 21, which were acquired after ion-milling ~100 nm into the substrate. The micrographs show different areas of the same surface. It can be seen that the porous domains in Fig. 21a are at various stages of development. In Fig. 21b, taken from a different area of the same sample, it can be seen that some domain merging has occurred (bottom left) and domains that are at very early stages of growth are also evident.

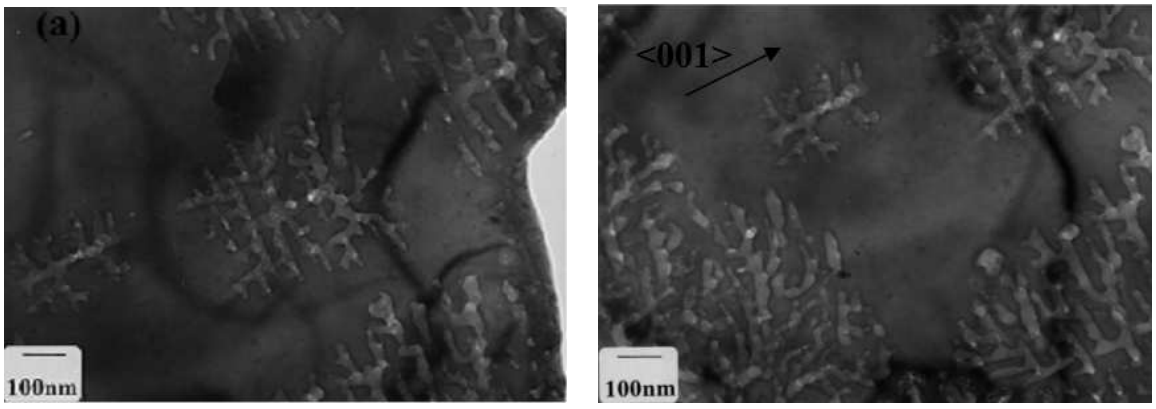


Fig. 21 Plan view bright field TEM images of a section through a porous InP layer ~100 nm below the surface of the electrode. Anodization conditions were the same as in Fig. 17. The plane of the micrograph is (100). Adjacent porous domains are visible.

From the AFM observations, the estimated surface pit density is 2.3×10^{7} cm^{-2}. Assuming that each pit forms a square based pyramidal domain and that their bases eventually cover the whole area of the electrode, the average area of the base of a domain is $1/(2.5 \times 10^{7}\ \text{cm}^{-2}) = 2 \times 10^{-8}$ cm^{2}. Thus the side is $(2.8 \times 10^{-8}\ \text{cm}^{-2}) = 2\ \mu$m. This is at least in order of magnitude agreement with the observed size of the domains, when they begin to touch (Figs. 17b and 21).

Because these observations have shown that the formation of individual porous domains beneath the surface of the semiconductor are linked to the formation of pits on the surface, *i.e.* that each domain stems from a surface pit, it follows then, that the development of the overall porous region occurs due to the merging of the progressively

nucleated porous domains. To examine this, the cross-sections of InP electrodes were examined by TEM following potential sweep anodization in 5 mol dm^{-3} at 2.5 mV s^{-1} from 0.0 V to 0.48 V (*i.e.* the current peak). Fig. 22 shows a resulting cross-sectional TEM micrograph. This micrograph suggests that the development of the porous layer is as a result of merging porous domains. It can be seen that merging of porous domains has occurred resulting in some sections of the porous region becoming fully formed.

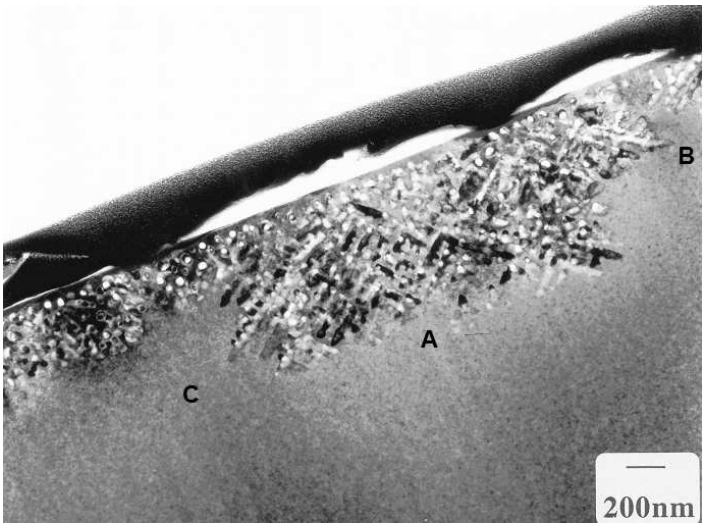


Fig. 22 Cross-sectional bright field TEM micrographs of n-InP after a potential sweep from 0.0 V to 0.48 V (SCE) at a scan rate of 2.5 mV s^{-1} in 5 mol dm^{-3} KOH electrolyte. The plane of the micrograph is (011).

The regions marked 'A' and 'B' are shown in a higher magnification image in Fig. 23. Fig. 23a shows a relatively homogeneous porous region ~700 nm in thickness. However, Fig. 23b obtained at another part of the same electrode (representing area 'B' in Fig. 22) clearly shows the merging of two porous domains. This micrograph shows that, at this stage of the anodization, not all of the nucleated porous domains have fully grown and merged.

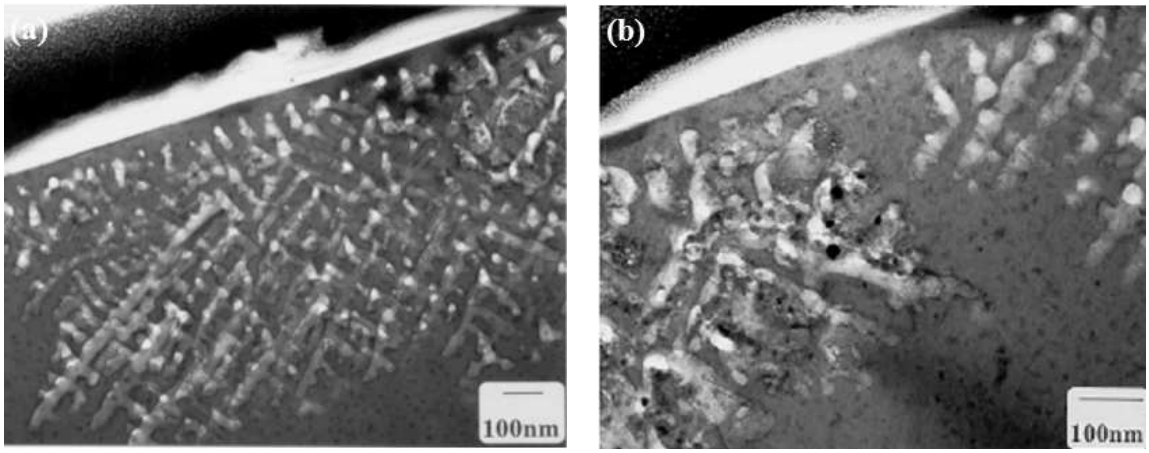


Fig. 23 Cross-sectional bright field TEM showing (a) region A and (b) region B in Fig. 22. The merging of two porous domains is evident in (b). The plane of the micrographs is (011).

The progressive formation of square-based pyramidal shaped porous domains from beneath etch pits on the surface is shown conclusively in Fig. 24a, which is a plan view TEM micrograph of the surface after potential sweep anodization similar to that described for Fig. 17b. Numerous domains are visible and some are noted to be considerably more developed than others. Furthermore, in some areas, considerable domain merging has occurred. In Fig. 24b, a cross-sectional TEM of the electrode anodized under the same conditions is shown. This image was acquired from a region where domains are seen to merge. The image suggests that a number of pyramidal porous domains are overlapping. Furthermore, direct evidence for the presence of a channel in the near-surface layer at the center of the pyramidal base is evident at 'A' in Fig. 24b. Thus, at the earlier stages of the anodic formation of porous InP in 5 mol dm^{-3} KOH, TEM clearly shows individual porous domains which appear triangular in cross-section and square in plan view.

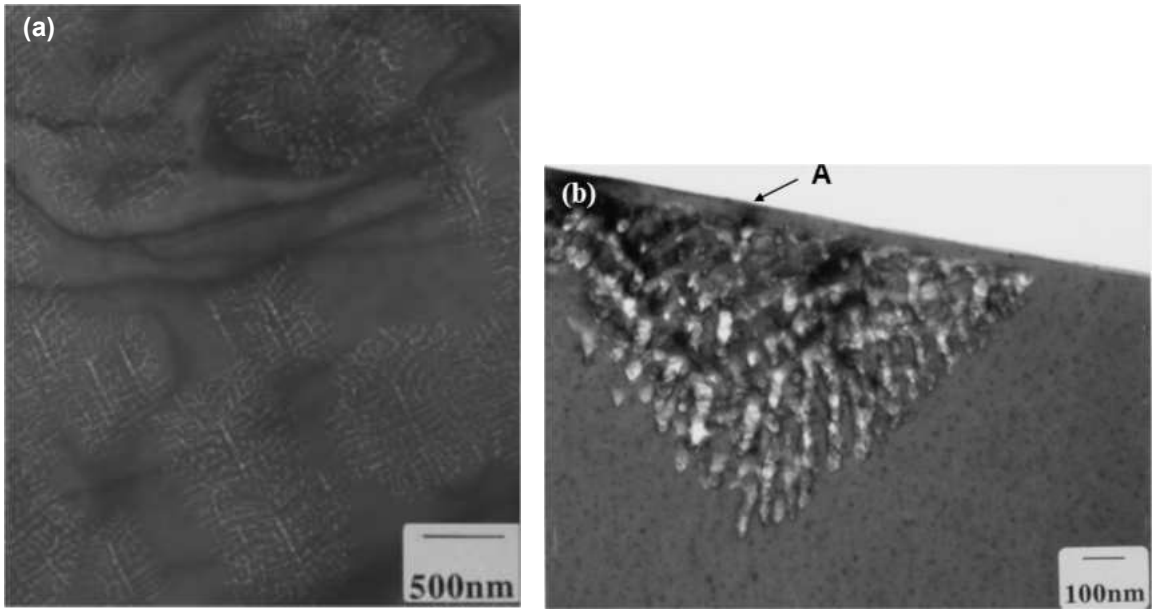


Fig. 24 (a) Plan view bright field TEM of n-InP after a potential sweep from 0.0 V to 0.48 V 18 (SCE) at a scan rate of 2.5 mV s^{-1} in 5 mol dm^{-3} KOH electrolyte. The progressive development of the porous domains is apparent. (b) cross-sectional (011) projection of the same electrode as in (a) showing merged pyramidal porous domains. An etch pit on the surface is observed in cross-section at 'A'.

The cross-sections also show that the domains are separated from the surface by a ~40 nm thick, dense InP near-surface layer. It has been shown that the porous domains have a square-based pyramidal shape and that each one develops from an individual surface pit, which forms a channel through this near-surface layer. We suggest that the pyramidal structure arises as a result of preferential pore propagation along the <100> directions.

Analysis of the cyclic voltammograms of InP electrodes in 5 mol dm^{-3} KOH indicates that, once a critical potential for pore formation is reached, the anodic current is predominantly time dependent and there is little differential dependence of the current on potential. [26] Modeling of the pore growth mechanism based on this evidence strongly suggests that our hypothesis is largely correct. The details of the numerical simulation are outlined in section 3.

3. Numerical Simulation of Porous Layer Growth

3.1 Porous Domain Formation

The process of porous growth in anodically etched n-type InP in 5 mol dm^{-3} KOH during the application of a potentiostatic voltage was modeled numerically. A mechanism of directional selectivity of pore growth preferentially along the <100> lattice directions was simulated and the results from these simulations were compared against experimental data. Experimentally pore growth creates nanoporous regions beneath a thin dense near-surface layer. In the early stages these regions take the form of square-based pyramidal domains originating at individual surface pits. Details of the numerical model employed can be found elsewhere. [28]

In Fig. 25, a typical porous structure formed initially during etching, in 5 mol dm^{-3} KOH is compared with a simulated structure created by the model. As expected, there is a strong resemblance between the initial porous domains formed experimentally and the structures that are simulated. The structures start from surface pits and grow along the <100> directions forming square-based pyramidal domains. The high potential at each of the pore tips allows pores to grow along all the <100> directions at an instantaneously equal rate causing regular domains to form and the number of active pore tips to increase rapidly. As these domains increase in size the concentration of electrolyte at the pore tips cannot be sustained by the diffusion of electrolyte from the surface pits and along the pores slowing down pore growth. The increase in the number of growing pore tips also increases the ohmic drops along the domain's pores.

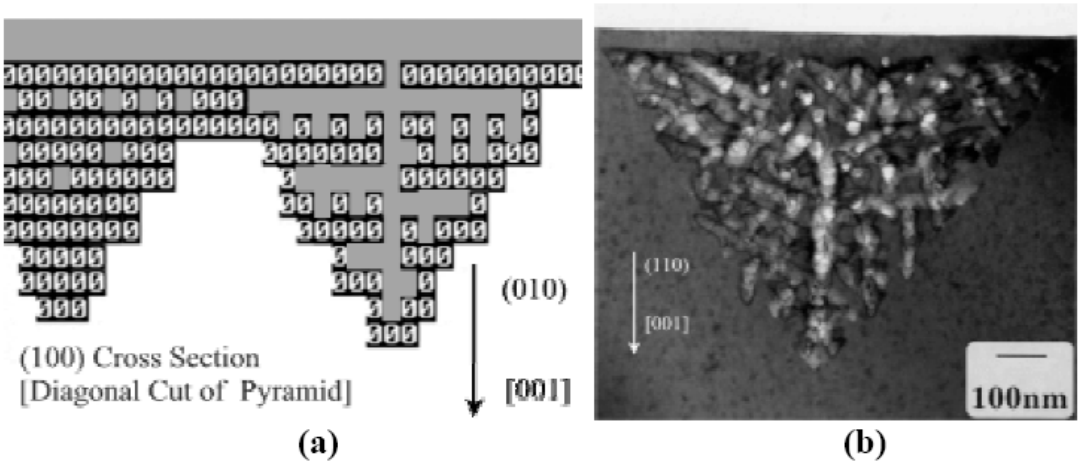


Fig. 25 (a) Initial structure formed prior to peak in current by a typical numerical simulation at an applied potential of 0.45 (KEY: 0 = InP depleted of carriers, White = Bulk InP, Grey = Pore) and (b) corresponding structure formed by electrochemical etching of InP during a linear potential seep from 0.0 V to 0.44 V in 5 mol dm^{-3} KOH at 2.5 mV s^{-1}. (from Ref. 28)

Different pore tips experience different ohmic drops which change continuously as the growth of new pores begin and end therefore with increasing domain size the ohmic drops experienced cause a greater spread of tip potentials. The effect of lower potentials with a wider distribution causes a range of low probabilities to be distributed at the pore tips producing a non-equal instantaneous growth rate and allowing the domains to lose their regular shape. At extended durations of etching, after the merging of the porous domains, this non-equal instantaneous growth rate allows for the formation of a

relatively flat porous to bulk interface similar to that found experimentally. These structures are created by the merging of porous domains after extended durations of etching.

3.2 Diffusion Controlled Pore Growth

When simulations at the same applied potential parameter but different diffusion coefficients are compared a shortening in the number of time-steps before the peak in current, is observed, for lower electrolyte diffusion coefficients. [28] Examination of these curves (cf. Fig. 1) explains the experimental behavior of current during initial etching. The initial rapid increase in current is caused by an expansion in the number of active pore tips as the domains spread out from the surface pits (as seen in Fig. 25). The current then peaks once the diffusion rate of electrolyte is no longer capable of sustaining the concentration at the pore tips above the threshold value for growth resulting in retardation in the growth of new pores. This can be concluded as the lowering of the diffusion coefficient causes the peaks to be limited to lower values of current and to occur at earlier times. The currents then decrease rapidly until a sustainable diffusion-consumption rate is attained producing a current that continues to gradually decrease as the average pore length increases. Diffusion of electrolyte is therefore a major controlling factor for pore growth rate and current: an increase in diffusion coefficient causes current peaks to increase in height, broaden and shift to later times and current values at extended durations to increase. It can also observed that at sufficiently high diffusion coefficients the current becomes limited by the ohmic resistance rather than by the diffusion rate of electrolyte along the pores.

It has been observed experimentally that below a threshold electrolyte concentration of 1.5 mol dm^{-3} KOH porous growth does not occur and instead the formation of thin oxide films on the InP surface is observed. [25,29]

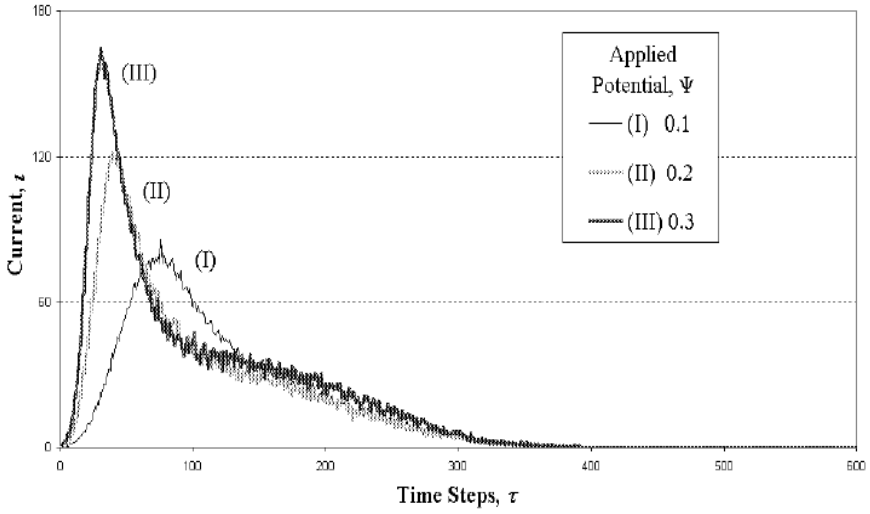


Fig. 26 Typical current versus time curves simulated for three different values of constant potential. The algorithm used allows for the termination of etching at pore tips by gradual irreversible modification of the active pore sites at electrolyte concentrations below the minimum concentration for pore growth. (from Ref. 28)

The electrolyte concentrations in pores eventually drop below this threshold that could lead to the partial filling of the pores with oxide, reducing the diffusion rate of

electrolyte. It is possible that the modification of the pore tips by low electrolyte concentrations may be permanent, stopping pore growth from recovering even when higher electrolyte concentrations are regained. The simulated curves for such a mechanism of termination are shown for three different values of constant potential in Fig. 26a and are in strong agreement with typical experimental curves shown in section 1.4 (Fig. 8). Both the experimental and simulated curves display currents that initially peak after different times before decreasing suddenly so as to merge and fall off gradually to very low currents at extended durations.

CONCLUSIONS

Potentiodynamic anodization of n-InP in a KOH electrolyte at concentrations of 2 mol dm^{-3} or greater results in selective etching of InP and the formation of a porous InP layer near the surface of the electrode. A linear sweep voltammogram of an n-InP electrode in these electrolytes shows a pronounced anodic peak. Cross-sectional TEM examination of electrodes, which have undergone such a sweep at 2.5 mV s^{-1} to a potential just past the peak, show an ~1 μm porous region just below the surface. A non-porous region, ~40 nm in thickness, remains at the surface of the electrode with the porous layer immediately underneath it. Potentiostatic anodization of n-InP electrodes at 0.5 - 0.75 V in 2, 3 and 5 mol dm^{-3} KOH also results in the formation of porous InP structures. A relatively constant percentage porosity is maintained. A value of 1.13 μm C^{-1} cm^2 was obtained for the ratio of porous layer thickness to charge density from which an estimate of ~35% was obtained for the porosity. The thickness of the porous layer and the mean pore diameter are noted to decrease with increasing KOH concentration both under potentiostatic and potentiodynamic anodization. The origin of the dense near-surface layer has not been fully explained but it is suggested that it may arise from carrier depletion in the semiconductor.

Investigation of the earlier stages of the anodic formation of porous InP in 5 mol dm^{-3} KOH. TEM clearly shows individual porous domains which appear triangular in cross-section and square in plan view. It is concluded that the porous domains have a square-based pyramidal shape and that each one develops from an individual surface pit which forms a channel through this near-surface layer. It is suggested that the pyramidal structure arises as a result of preferential pore propagation along the <100> directions. Atomic force microscopy (AFM) measurements show that the density of surface pits increases with time. Each of these pits acts as a source for a pyramidal porous domain, and these domains eventually form a continuous porous layer. This implies that the development of porous domains beneath the surface is also progressive in nature. Evidence for this was seen in plan view TEM images. Merging of domains continues to occur at potentials more anodic than the peak potential, where the current is observed to decrease. When the domains grow, the current density increases correspondingly. Eventually, domains meet, the interface between the porous and bulk InP becomes relatively flat and its total effective surface area decreases resulting in a decrease in the current density.

The numerical current versus time curves produced also exhibit good agreement with experimental data. Manipulation of the parameters controlling these curves shows that the fall-off in current is controlled by the rate of diffusion of electrolyte through the pore structure with the final decline in current being caused by the termination of growth at the pore tips through the formation of passivating films or some other irreversible modification of the pore tips.

REFERENCES

[1] L.T. Canham, *Appl. Phys. Lett.*, **57**, 1046 (1990)
[2] H. Föll, *Appl. Phys. A*, **53**, 8 (1991)
[3] T. Holec, T. Chvojka, I. Jelínek, J. Jindřich, I. Němec, I. Pelant, J. Valenta and J. Dian, *Mater. Sci. Eng. C*, **19**, 251 (2002)
[4] R.J. Martín-Palma, J.M. Martínez-Duart, L. Li and R.A. Levy, *Mater. Sci. Eng. C,* **19**, 359 (2002)
[5] A. Matoussi, T. Boufaden, A. Missaoui, S. Guermazi, B. Bessaïs, Y. Mlik and B. El Jani, *Microelectronics Journal,* **32**, 995 (2001)
[6] A. Jain, S. Rogojevic, S. Ponoth, N. Agarwal, I. Matthew, W.N. Gill, P. Persans, M. Tomozawa, J.L. Plawsky and E. Simonyi, *Thin Solid Films,* **398**, 513 (2001)
[7] N.E. Chayen, E. Saridakis, R. El-Bahar, Y. Nemirovsky, *J. Molec. Biol.,* **312**, 591 (2001)
[8] S. Langa, J. Carstensen, M. Christophersen, H. Föll, and I.M. Tiginyanu, *Appl. Phys. Lett.*, **78**, 1074 (2001)
[9] G. Oskam, A. Natarajan, P.C. Searson and F.M. Ross, *Appl. Surf. Sci.*, **119**, 160 (1997)
[10] M.M. Faktor, D.G. Fiddyment and M.R. Taylor, *J. Electrochem. Soc.*, **122**, 1566 (1975)
[11] F.M. Ross, G. Oskam, P.C. Searson, J.M. Macaulay and J.A. Liddle, *Philos. Mag. A*, **75**, 2 (1997)
[12] C. O'Dwyer, D.N. Buckley, V.J. Cunnane, D. Sutton, M. Serantoni and S.B. Newcomb, in *Proceedings of the State-of-the-Art Program on Compound Semiconductors XXXVII*, **PV 2002-14**, p. 259, The Electrochemical Society, Proceedings Series, Pennington, NJ (2002)
[13] S. Langa, J. Carstensen, I.M. Tiginyanu, M. Christophersen and H. Föll, *Electrochem. Solid-State Lett.*, **4**, G50 (2001)
[14] S. Langa, I.M. Tiginyanu, J. Carstensen, M. Christophersen and H. Föll, *Electrochem. Solid-State Lett.* **3**, 514 (2000)
[15] E. Harvey, C. O'Dwyer, T. Melly, D.N. Buckley, V.J. Cunnane, D. Sutton, S.B. Newcomb and S.N.G. Chu, in *Proceedings of the State-of-the-Art Program on Compound Semiconductors XXXV*, P.C. Chang, S.N.G. Chu, and D.N. Buckley, Editors, **PV 2001-2**, p. 87, The Electrochemical Society, Proceedings Series, Pennington, NJ (2001)
[16] P. Schmuki, J. Fraser, C.M. Vitus, M.J. Graham, H.S. Isaacs, *J. Electrochem. Soc.*, **143**, 3316 (1996)
[17] P. Schmuki, D.J. Lockwood, J. Fraser, M.J. Graham, H.S. Isaacs, *Mater. Res. Soc. Symp. Proc.,* **431**, 439 (1996)
[18] M. Christopherson, J. Carstensen, A. Feuerhake and H. Föll, *Mater. Sci. Eng. B*, **69**, 70, 194 (2000)
[19] S. Rönnebeck, J. Carstensen, S. Ottow and H. Föll, *Electrochem. Solid-State Lett.*, **2**, 126 (1999)
[20] P. Schmuki, L.E. Erickson, D.J. Lockwood, J.W. Fraser, G. Champion, H.J. Labbé, *Appl. Phys. Lett.*, **72,** 1039 (1998)
[21] B.H. Erne, D. Vanmaekelbergh and J.J. Kelly, *J. Electrochem. Soc.*, **143**, 305 (1996)
[22] J. Carstensen, M. Christophersen and H. Föll, *Mater. Sci. Eng., B*, **69-70**, 23 (2000)
[23] S. Langa, J. Carstensen, I.M. Tiginyanu, M. Christophersen and H. Föll, *Electrochem. Solid-State Lett.*, **5**, C14 (2002)

[24] C. O'Dwyer, D. N. Buckley, D. Sutton and S. B. Newcomb, in *Proceedings of the State-of-the-Art Program on Compound Semiconductors XXXVIII*, E.B. Stokes, R.C. Fitch, D.N. Buckley, P.C. Chang, Y. Koide, R.F. Kopf, F. Ren, R.E. Sah, P.H. Shen, and D.M. Walker, Editors, **PV 2003-04**, p. 63, The Electrochemical Society, Proceedings Series, Pennington, NJ (2003)
[25] D.N. Buckley, C. O'Dwyer, E. Harvey, T. Melly, D. Sutton and S.B. Newcomb, (*invited)* in *Proceedings of the State-of-the-Art Program on Compound Semiconductors XXXVIII*, E.B. Stokes, R.C. Fitch, D.N. Buckley, P.C. Chang, Y. Koide, R.F. Kopf, F. Ren, R.E. Sah, P.H. Shen, and D.M. Walker, Editors, **PV 2003-04**, p. 48, The Electrochemical Society, Proceedings Series, Pennington, NJ (2003)
[26] C. O'Dwyer, D.N. Buckley, M. Serantoni, D. Sutton and S.B. Newcomb, in *Proceedings of the State-of-the-Art Program on Compound Semiconductors XXXIX*, R.F. Kopf, D.N. Buckley, F. Ren, C. Monier, K. Shiojima, A.G. Baca, H.M. Ng, T.D. Moustakas, S.J. Pearton, Editors, **PV 2003-11**, p. 136, The Electrochemical Society, Proceedings Series, Pennington, NJ (2003)
[27] *CRC Handbook of Chemistry and Physics*, 81st ed., D.R. Lide Editor, CRC Press, NY (2000)
[28] R. Lynch, C. O'Dwyer, I. Clancy, D. Corcoran and D.N. Buckley, in *Proceedings of the State-of-the-Art Program on Compound Semiconductors XXXIX*, **PV 2004-6**, p. 85, The Electrochemical Society, Proceedings Series, Pennington, NJ (2004)
[29] C. O'Dwyer, T. Melly, E. Harvey, D.N. Buckley, V.J. Cunnane, D. Sutton, M. Serantoni and S.B. Newcomb, in *Proceedings of the State-of-the-Art Program on Compound Semiconductors XXXVII*, P.C. Chang, W.K. Chan, D.N. Buckley, A.G. Baca, Editors, PV 2002-14, p. 233, The Electrochemical Society, Proceedings Series, Pennington, NJ (2002)